Cation Ordering and Oxygen Release in $LiNi_{0.5-x}Mn_{1.5+x}O_{4-y}$ (LNMO): *In-situ* Neutron Diffraction and Performance in Li-ion Full Cells

Burak Aktekin[1], Mario Valvo[1], Ronald I. Smith[2], Magnus H. Sørby[3], Fernanda Lodi Marzano[4], Wolfgang Zipprich[5], Daniel Brandell[1], Kristina Edström[1], William R. Brant[1*]

[1]*Department of Chemistry – Ångström Laboratory, Uppsala University, Box 538, SE-75121, Uppsala, Sweden*
[2]*ISIS Pulsed Neutron and Muon Source, Rutherford Appleton Laboratory, Harwell Campus, Didcot, OX11 0QX, UK ISIS*
[3]*Department for Neutron Materials Characterization, Institute for Energy Technology, P.O. Box 40, NO-2027, Kjeller, Norway*
[4]*Scania CV AB, SE-151 87, Södertälje, Sweden*
[5]*Volkswagen AG, D-38436, Wolfsburg, Germany*
**william.brant@kemi.uu.se*

Abstract

Lithium ion cells utilising $LiNi_{0.5}Mn_{1.5}O_4$ (LNMO) as the positive electrode are prone to fast capacity fading, especially when operated in full cells and at elevated temperatures. The crystal structure of LNMO can adopt a $P4_332$ (cation ordered) or Fd-3m (disordered) arrangement, and the fading rate of cells is usually mitigated when samples possess the latter structure. However, synthesis conditions leading to disordering also lead to oxygen deficiency, rock-salt impurities and as a result generate Mn^{3+}. In this study, *in-situ* neutron diffraction was performed on disordered and slightly Mn-rich LNMO samples to follow cation ordering-disordering transformations during heating and cooling. The study shows for the first time that there is not a direct connection between oxygen release and cation disordering, as cation disordering is observed to start prior to oxygen release when the samples are heated in a pure oxygen atmosphere. This result demonstrates that it is possible to tune disordering in LNMO without inducing oxygen deficiencies or forming the rock-salt impurity phase. In the second part of the study, electrochemical testing of samples with different degrees of ordering and oxygen content have been performed in LNMO‖LTO ($Li_4Ti_5O_{12}$) full cells. The disordered sample exhibits better performance as has been reported by other studies, however, we observe that all cells behave similarly during the initial period of cycling even when discharged at 10C rate, while differences arise only after a period of cycling. Additionally, the differences in fading rate were observed to be time dependent rather than dependent on the number of cycles. This performance degradation is believed to be related to instabilities of LNMO at higher voltages, that is, in its lower lithiation states. Therefore, it is suggested that future studies should be targeted at studying the individual effect of ordering and oxygen content. It is also suggested that more emphasis during electrochemical testing should be put on the stability of samples in their delithiated state.

Keywords: *High voltage spinel, neutron diffraction, LNMO, cation ordering, oxygen deficiency*

Introduction

$LiNi_{0.5}Mn_{1.5}O_4$ (LNMO) is a promising spinel-type positive electrode (cathode) material for lithium-ion batteries (LiBs), with a theoretical capacity of 147 mAh/g and an operating voltage around 4.7 V (vs. Li/Li^+). This voltage plateau at 4.7 V (vs. Li/Li^+) is due to the active Ni^{2+}/Ni^{4+} redox couple, while a second (minor) plateau around 4.1 V (vs. Li/Li^+) due to the Mn^{3+}/Mn^{4+} redox couple can be present depending on the synthesis conditions.[1] In addition to energy gain from high voltage, the spinel crystal structure possesses 3-D pathways for the lithium diffusion.[2] As the electronic conductivity of LNMO is also sufficiently high (10^{-5} – 10^{-7} S/cm)[3], it is thus regarded as a suitable cathode material also for high power applications (e.g. electric vehicles), even when micron-sized powders are used.[4] However, commercialization of LMNO-based cells is held back due to fast capacity fading in full cells, especially at elevated temperatures.[5] It is known that synthesis-related factors may have a significant impact on its

fast capacity fading. These factors might be related to the degree of cation ordering,[6,7] oxygen deficiency,[8,9] formation of impurity phases,[8,10] particle morphology,[11,12] etc. Therefore, for the purpose of developing LNMO-based cells with long lifetimes, it is important to identify the relationship between those mentioned material properties and their role on the electrochemical performance.

The thermodynamically favoured crystal structure (at room temperature) of LNMO crystallises in a structure with $P4_332$ symmetry.[13] In this structure, Mn and Ni cations occupy specific atomic sites (12d and 4a, respectively) and this phase is therefore usually referred to as the ordered phase. In addition, Li atoms are located at 8c while O atoms are at 24e and 8c sites.[14] Alternatively, the kinetically favoured structure has a higher symmetry and is represented by the *Fd*-3*m* space group. Mn and Ni cations occupy 16d sites randomly while Li atoms are at 8a and O atoms at 32e sites.[14] This phase is referred to as the disordered phase. High temperature calcination (>750˚C) during the synthesis of LNMO has been reported to yield the disordered phase (*Fd*-3*m*)[2,9,15] while an additional annealing step around 700˚C followed by slow cooling is necessary to obtain ordered LNMO with the $P4_332$ space group.[7,15,16] In literature, even though it is common to report synthesized powders as either of these two structures, it is important to note that the synthesis of perfectly ordered or disordered phases can be hard to achieve practically,[17] and partial ordering-disordering of varying degrees likely exists.[18] It should be noted at this point that these two structures reported in the literature represent the bulk average structure of LNMO (e.g. as determined by diffraction techniques) while an ordered arrangement of Mn/Ni can still exist in the local structure (lattice-cell) of fully disordered phase.[19]

The conditions that favor the disordered phase (i.e. high temperatures) are also known to cause oxygen loss from the structure.[20,21] The oxygen release starts at temperatures above 700˚C and reaches significant levels at 730˚C during heating in air, in close proximity with the synthesis temperature which also favors the disordered phase.[20] At higher temperatures, further oxygen loss is accompanied by the formation of rock-salt phase impurities (>750˚C), however, this phase can reversibly transform back to the spinel phase during cooling as long as the cooling is sufficiently slow.[15] Compositions with varying stoichiometry have been reported for the rock-salt phase, e.g. NiO,[15] $Li_xNi_{1-x}O$,[22] $(Li_{1/3}Mn_{1/2}Ni_{1/6})_xO$[21] and $(Li_xMn_{0.66}Ni_{0.34})_yO$.[10] In summary, it is thus likely that the 'disordered' LNMO electrodes reported in the literature might actually have partial cation ordering, varying degrees of oxygen deficiency, impurity phases and deviations from the stoichiometric formula, i.e. deviations in Mn/Ni ratio and oxygen occupancy.

Considering such variations that might originate during synthesis, it is reasonable that the 'ordered' and 'disordered' LNMO display diverse electrochemical performance in many studies. Additionally, possible changes in particle shape and size could increase the complexity even further. Nevertheless, a majority of studies agree on better cycling stability and rate capability of 'disordered' electrodes[2] although, the exact reasons behind this improvement are still unclear. Understanding the core reason for material performance improvement becomes even more important as some characteristics of the 'disordered' LNMO are not desired. For instance, ordered LNMO, with its ideal stoichiometry of $LiNi_{0.5}Mn_{1.5}O_4$, compensates the charge neutrality via the Ni^{2+}/Ni^{4+} redox couple during lithiation/delithiation while the Mn oxidation state (4+) remains constant. Therefore, a single voltage plateau around 4.7 V (vs. Li/Li^+) is observed.[23] Disordered LNMO, on the other hand, consists of some amount of Mn^{3+} which is oxidized to Mn^{4+} state at the beginning of charging, thereby causing the voltage plateau around 4.1 V (vs. Li/Li^+).[23] This is not desirable as the decrease in voltage reduces the energy density. Moreover, the presence of Mn^{3+} can favor the formation of Mn^{2+} via disproportionation ($2Mn^{3+} \rightarrow Mn^{2+} + Mn^{4+}$) on the particle surface, resulting in dissolution of Mn^{2+} into the electrolyte and a decrease in the cell life time.[5,24] Despite this, some Mn^{3+} is still desired as it is believed to be responsible for the better cycling performance of the disordered phase, e.g. increased electronic conductivity.[3] This conception has been challenged in some recent studies. For instance, when electronic conductivities were investigated as a function of lithiation state, significantly higher electronic conductivity for the disordered sample was indeed observed, but only at the beginning of charging. The conductivities were comparable for most of the cycling period, where Mn^{3+} was absent.[4,25]

The difference in electrochemical performance can also be due to phase transformations occurring during cycling. For the ordered LNMO, during charging (delithiation) and discharging (lithiation), two

successive 'two-phase transformations' are observed through three cubic phases.[7,17,25,26] For the disordered LNMO, not only two-phase reactions are present; but also a solid solution behavior is observed (at high lithiation states). This causes a reduction of two-phase transformation domains.[17] This would decrease the mechanical strain caused by coexisting phases and reduce the kinetic barriers caused by nucleation and growth processes.[27] Therefore, as an alternative explanation, the presence of solid-solution regions in the disordered phase may be the reason of its better electrochemical performance, rather than the Mn^{3+} presence.

In literature, even though some studies suggested beneficial effect of disordering over Mn^{3+} presence,[28] there has been no dedicated study with an aim to understand individual effect of these two properties using proper set of samples. Therefore, it still remains unclear if the disordering in the structure, or the oxygen loss during synthesis is responsible for the enhanced electrochemical performance of 'disordered' LNMO. Additionally, given that the use of terms 'ordered' and 'disordered' for samples are not well-defined, variations in experimental results are observed[17] since the use of these terms often discards other material properties such as oxygen content and neglects the partial degrees of ordering. This makes understanding the origins of difference in electrochemical performance harder. Ideally, it would be easier to achieve such an understanding if it was possible to synthesize and test a cation disordered LNMO without the presence of Mn^{3+}. In order to explore such a possibility further, it is first necessary to understand how Mn^{3+} is introduced into the structure and how it is linked with the cation disordering. In that way, it could be possible to obtain samples with different ordering and Mn^{3+} content and thus test their individual effect.

Following the oxygen release during heating, Mn^{3+} can be introduced into the structure in different ways. By creation of oxygen vacancies in the structure, some Mn^{3+} is generated in order to maintain charge neutrality.[21] Alternatively, Cabana *et al.* reported that a rock-salt phase with a lower Mn/Ni ratio (Ni-rich) can be formed following oxygen release at high temperature.[10] This increases the Mn/Ni ratio in the spinel phase, thus introducing Mn^{3+} without oxygen vacancy requirement. In either case, the presence of Mn^{3+} (65 pm) can favor cation disordering as a result of its larger ionic radius (vs. 54 pm for Mn^{4+}) that is comparable to the Ni^{2+} (69 pm) radius.[20] In other words, oxygen release and subsequent Mn^{3+} formation can be said to favour disordering.

In a recent theoretical study, it was suggested that formation of oxygen vacancies would decrease the energy of the disordered structure.[29] Therefore, during heating, onset of cation disordering could favour the oxygen release instead, rather than the other way around. In all scenarios, if there is a direct relation between disordering and the oxygen release, this would render the individual role of disordering on the electrochemical behavior complex to isolate. It is also clear that, depending on the nature of this relation, cooling conditions can play an important role (e.g. due to kinetics of re-ordering, oxygen uptake and rock-salt elimination).[30] Therefore, in exploring these relations, *in-situ* characterizations of structure can be highly useful compared to *ex-situ* characterization of samples 'quenched' from different temperatures.

In this study, in order to gain further insight on cation ordering and its effect on electrochemical behaviour, we use *in-situ* neutron diffraction (ND) to follow ordering transitions during the heating/cooling of LNMO powders. The use of neutron diffraction is necessary for an accurate characterization of cation ordering, as Mn and Ni have very similar scattering powers with X-ray diffraction, whereas with neutrons they are very different enabling accurate identification of $P4_332$ and *Fd*-3*m* structures.[31] So far, there have been only two important studies which have investigated ordering transitions via *in-situ* ND techniques. Pasero *et al.* studied heating of LNMO under vacuum[21] and Cai *et al.* under air atmosphere.[15] Here, with an effort to understand relationship between ***'disordering ↔ oxygen release ↔ presence of Mn^{3+}'***; we perform *in-situ* heating/cooling characterization of slightly Mn-rich LNMO under pure oxygen atmosphere, for the first time, using ND. It could be expected that the increasing oxygen partial pressure would shift the onset of oxygen release to higher temperatures. Therefore, if there is a direct relation between oxygen release and cation disordering, the ordering-disordering transition temperature (T_{O-D}) would also shift accordingly. Furthermore, instead of stoichiometric LNMO (Mn/Ni = 3), we used slightly Mn-rich LNMO (Mn/Ni = 3.5), making sure there was always some Mn^{3+} present in the structure being independent of the temperature. As mentioned

earlier, Mn/Ni ratio can increase during the heat treatment even if this ratio is 3 at the beginning. Therefore, having excess Mn would reduce the sensitivity towards the effects of Mn/Ni compositional changes in the spinel. Additionally, Mn-rich samples would be expected to show less tendency towards rock-salt phase formation[8] and this would help further in reducing the risk of Mn/Ni ratio change. Lastly, if there is a direct relation between the Mn^{3+} content and the tendency to disordering, a shift of T_{O-D} to lower temperatures would be expected as large Mn^{3+} atoms would disrupt the structure and facilitate disordering. As a result, these conditions would enable a less complicated experiment to observe the relationship between 'disordering ↔ oxygen release ↔ presence of Mn^{3+}'. In the second part of the study, 'ordered' and 'disordered' samples were prepared by careful annealing/cooling of powders without introducing the impurity phase and without changing the particle morphology. After characterization of oxygen content and cation ordering, electrochemical performance of these samples are tested in full cells using $Li_4Ti_5O_{12}$ (LTO) as the negative electrode, which is known for its electrochemical and structural stability.[32] Using this cell chemistry, it is possible to get useful information on cycling stability and power capability of LNMO electrodes.[33]

Experimental

Sample preparation. Micron-sized commercial LNMO powders were used as reference samples. In order to obtain disordered LNMO, powders were heated up to 800˚C and annealed for 12 hours in air and then quenched to room temperature (by water quenching the alumina crucible). For ordered samples, LNMO powders were heated to 600˚C and annealed for 12 hours under pure oxygen (atmospheric pressure). Later, powders were cooled down to 300˚C slowly in 12 hours, where after the furnace was cooled to room temperature. It should be noted that the use of submicron-scaled powders would not be suitable as particle size and shape would also tend to change during heat treatment.

***In-situ* characterization.** *In-situ* neutron diffraction data were collected on the POLARIS medium resolution time-of-flight (TOF) powder diffractometer at the ISIS spallation neutron source, Rutherford Appleton Laboratory (RAL), UK.[34] Approximately 2 grams of powdered sample were loaded into a reaction cell manufactured from 316 stainless steel (inner diameter 11mm; wall thickness 0.2mm) capable of allowing a flow of gas through the sample. The cell was placed into a RAL-designed neutron diffraction furnace (comprising a heating element and heat shields made from vanadium foil) mounted on the diffractometer. The in situ reaction cell incorporates a collimating mask made from neutron-absorbing boron nitride ceramic and gadolinium foil, making it possible to collect diffraction patterns in the Polaris 90˚ detector bank ($83^\circ < 2\theta < 97^\circ$, dmax = 4.0 Å, $\delta d/d = 0.70\%$) which are free of Bragg reflections from the steel reaction cell itself. Gas flow through the cell was from bottom to top, with a coiled section in the inlet pipe allowing the flowing gas to heat to the furnace temperature and minimize any sample cooling effect due to the gas flow. A type K thermocouple located close to the outside of the collimation was used to control furnace temperature, with a second type K thermocouple inserted into a drilled hole in the top flange of the reaction cell used to monitor the resulting sample temperature. The temperature of this latter thermocouple is reported in the results. A disordered LNMO sample (see sample preparation section for details) was heated and cooled under pure oxygen flow (atmospheric pressure, around 1 bubble per 1-2 seconds in a Dreschel bottle) at different rates (1˚C/min and 2˚C/min). For every pattern, data collection time was 5 minutes and 257 patterns were collected in total. Sequential Rietveld refinement was performed on 257 patterns using the GSAS[35] suite of programs with graphical user interface EXPGUI.[36] Refinements were performed on data range 0.64 Å – 2.74 Å. The degree of ordering was quantified by allowing cation mixing in $P4_332$ structure.

Characterization of LNMO samples used in LNMO-LTO full cells. Reference and ordered samples were characterized *ex-situ* at room temperature on the constant wavelength (1.555 Å) powder neutron diffractometer PUS at the JEEP II reactor, Norway.[37] The data range was 10˚–130˚ (2-theta) and Rietveld refinements were made on the whole range, however, graphs were drawn in a smaller range in order to directly compare with the data from the POLARIS diffractometer. Thermal gravimetric analysis (TGA) analysis was performed under pure oxygen gas flow using Q500-TGA 1000˚C equipment from TA instruments. The maximum temperature was 780˚C and the sample holder was platinum. Raman

spectroscopy was performed through a Raman microscope (Renishaw – inVia) using an excitation wavelength of 532 nm provided by a solid-state laser (Renishaw) with a maximum power of 500 mW. Prior to the measurements, a calibration was carried out by means of a crystalline Si sample to ensure that a characteristic reference peak was obtained around 520.6 cm^{-1}. Twenty consecutive acquisitions with a nominal laser power of 0.5 mW and a measuring time of 20 s were run between 100 and 800 cm^{-1} to collect the spectra, while applying beam exposure minimization in between subsequent acquisitions to avoid possible surface degradation of the specimens. Inductively coupled plasma – optical emission spectroscopy (ICP-OES) was used for determining Mn/Ni ratio in the LNMO powders using PerkinElmer Optima 7300DV spectrometer. Sample was digested in aqua regia and diluted with deionized water. Measurement was performed via internal standard method (scandium) with two point calibration.

Electrochemical characterization. Positive electrodes consisting of LNMO powders (90 wt%) with carbon black (Imerys, C65, 5 wt%) and a poly(vinylidene difluoride)-based binder (5 wt%, PVdF-HFP, Kynar Flex 2801) were prepared. The average porosity was 40-50% after electrode calendaring. The capacity of LNMO electrodes were in the range of 1.5–1.6 mAh/cm^2. Commercial LTO electrodes (Leclanché) with a capacity of 1.7 mAh/cm^2 were used as counter electrodes. Less capacity for LNMO was intentionally chosen as LNMO-limited cells would immediately reflect cyclable lithium loss in this full cell chemistry.[33] In pouch cells, Celgard 2500 (two layers) was used as separator and 1 M $LiPF_6$ (Ferro Corp.) dissolved in EC:DEC (1:1 by volume, BASF) was used as electrolyte (120 µl per cell). More details of electrode and cell preparation are described in our earlier study.[33] Full cells were galvanostatically cycled between 1.5 V–3.5 V (vs. LTO) at varying rates. A Novonix HPC (High Precision Charger) system was used for testing of cells at 55˚C. All cells testing started with a 10 hours OCV period at 55˚C and unless stated, there was no constant voltage (CV) step nor pausing (at open circuit voltage, OCV) between charging–discharging.

Results and Discussions

***In-situ* analysis of $LiNi_{0.5-x}Mn_{1.5+x}O_{4-y}$ during heating/cooling.** It is known that LNMO starts releasing oxygen at elevated temperatures,[20] and it is also reasonable to expect that the onset of oxygen release should shift to higher temperatures under higher oxygen partial pressures. Therefore, *in-situ* neutron diffraction experiments were performed under pure oxygen flow (atmospheric pressure) in order to see if T_{O-D} is shifted accordingly. Disordered samples were first analyzed via TGA to verify the shift of oxygen release temperature. For this purpose, two identical samples were heated/cooled either under air or pure oxygen flow. As seen in Figure 1, the disordered samples start to take up oxygen when the temperature is above 400˚C. The oxygen uptake rate and the total amount of oxygen recovery are higher when heating under oxygen flow. When the temperature is increased further, this time oxygen release starts. Under air flow, oxygen release starts around 690-695˚C (temperature where the tangent to the weight vs. temperature on the graph is 45˚, or the slope is $-2.89 \times 10^{-5} \times {}^{\circ}C^{-1}$) while this temperature is shifted to 725-730˚C under oxygen. Therefore, it is verified that changing from air to pure oxygen atmosphere increases the onset of the oxygen release temperature around 35-40˚C. Oxygen occupancy in the LNMO chemical formula is also given on the right-y axis of the Figure 1 to demonstrate the relative amount of oxygen released. It should be noted that oxygen occupancy values are based on the assumption that oxygen release is compensated by vacancies on the oxygen site. It is also assumed that full oxygen occupancy (y=4) is reached at the point of maximum weight under oxygen flow. Values obtained for heating under air are in accordance with the values reported earlier.[21]

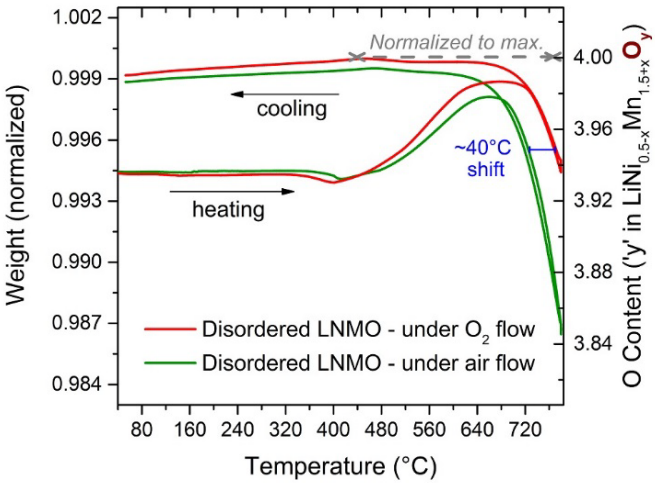

Figure 1. TGA analysis of disordered LNMO samples heated/cooled (1.5 ˚C/min) under air flow or oxygen flow. The maximum point in the case of oxygen flow was normalized to 1 (weight). On the right y-axis, corresponding oxygen stoichiometry is shown with the assumption that the oxygen-cooled sample is not oxygen deficient.

In a similar way, the disordered LNMO sample was heated and cooled under pure oxygen flow during the *in-situ* neutron diffraction experiment (1 or 2˚C/min rate vs. 1.5˚C/min rate during TGA). The heating/cooling was interrupted several times with isothermal steps to observe any effect of kinetic limitations during phase transitions. The sample first was heated up to 597˚C and kept at this temperature for 35 min to observe the progress of cation ordering. Later, the temperature was raised to 680˚C and kept similarly at this temperature for 56 min. It was followed by cooling and then isothermal treatment at 604˚C for 315 min. As a final step, the sample was heated up to 820˚C and cooled down to 494˚C. ND patterns are shown as a contour plot in Figure 2 where the temperature vs. time profile is also shown on the right-hand side of the plot.

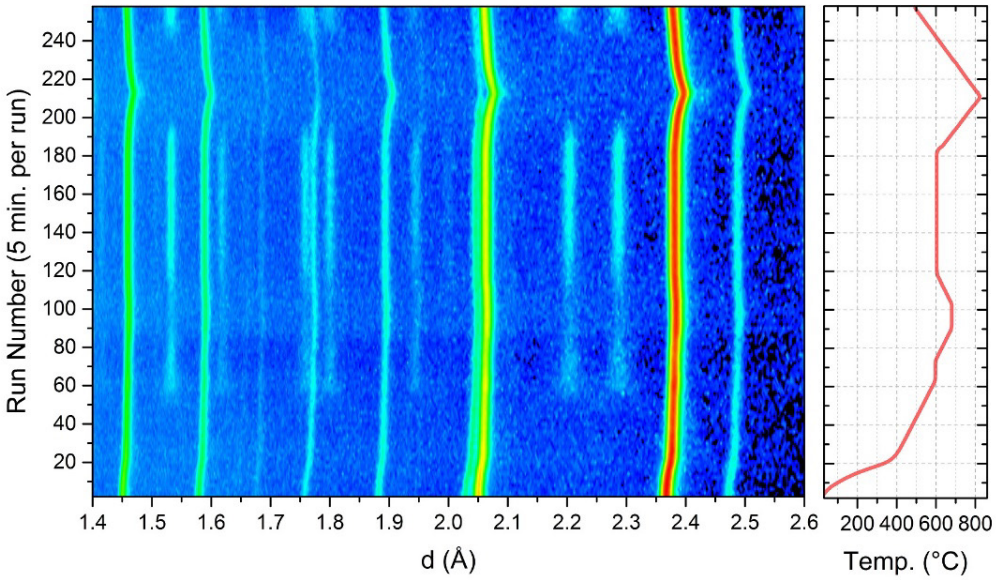

Figure 2. Neutron diffraction data for the heating/cooling of disordered LNMO powders under oxygen atmosphere. The intensity values are in arbitrary units.

Starting from the bottom of Figure 2, initially only the peaks of disordered LNMO (*Fd*-3*m*) are present except for some small peaks originating from the collimating mask (boron nitride ceramic and

gadolinium foil) at 1.76 Å and 2.03 Å (small contribution to the left tail of peak at 2.05 Å). As the sample is heated, peaks from the ordered structure ($P4_332$) begin to appear (around run number 50). During the isothermal step at 604˚C, those superlattice peaks reach their highest intensity indicating a high degree of ordering. Peak broadening also seems to decrease with increasing degree of ordering (see Figure S1 for selected patterns) as reported previously.[19,28] While cation ordering is easily observed, no visible peaks originating from a rock-salt impurity phase can be seen in Figure 2. In the study by Cai *et al.*, the formation of rock-salt phase was clearly visible above 750˚C through the appearance of new reflections, e.g. the rock-salt 220 reflection at 1.48-1.49 Å.[15] At 800˚C, both spinel and rock-salt peaks were present. In Figure 3, with an attempt to detect any traces of rock-salt phase formation, the data in Figure 2 are drawn with zoomed-in sections of 1.44-1.50 Å and 2.03-2.13 Å, where the two most intense peaks for the rock-salt phase are expected to be seen. Indeed, only a small trace of rock-salt phase appears at the very end of heating in the region 800-820˚C (e.g. at 1.486 Å and 2.095 Å, see Figure S2 for a single diffraction pattern at 820˚C). These small peaks disappear during subsequent cooling (with 2˚C/min rate). Nevertheless, it is clearly seen that both excess Mn in LNMO and pure oxygen environment make the material less prone to rock-salt phase formation during heating. This can be considered as an advantage since rock-salt phase would lower the charge capacity and possibly increase the ionic resistance.

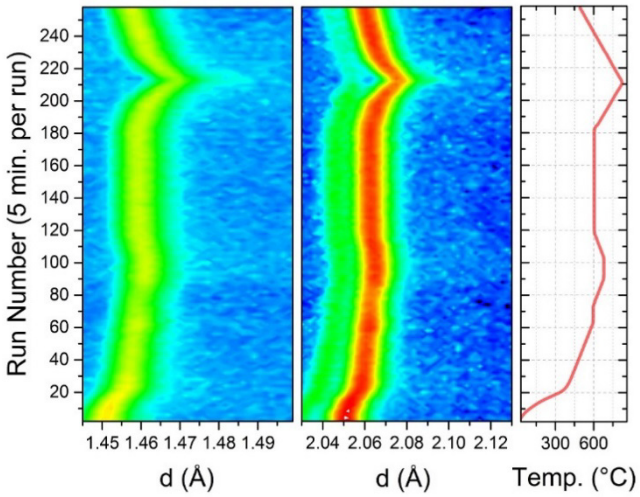

Figure 3. Zoom-in view of neutron diffraction data for d-spacing ranges of 1.44-1.50 Å and 2.03-2.13 Å where two most intense peaks for the rock-salt impurity phase (*Fm*-3*m*) would be expected to be visible. The intensity values are in arbitrary units.

To obtain more quantitative information from the *in-situ* neutron diffraction experiment, sequential Rietveld analysis has been performed on a total number of 257 patterns collected during the experiment. For the refinements, an ordered structure ($P4_332$) model with a fixed Mn:Ni ratio of 0.78:0.22 (based on ICP analysis) was applied for all temperatures. Li occupancy was fixed to 1.0. An attempt to refine O occupancy was also made, however, although the refined O occupancies were close to 1.0, estimated standard deviations (esds) on the refined parameters were much larger than the scatter in their values meaning that the changes observed in TGA analysis could not be detected. The accuracy of the O occupancy refinement was improved by merging multiple diffraction patterns collected during the isothermal step at 680˚C (56 min), but the change in O occupancy was again within the range of esds. Therefore O occupancy was also fixed to 1.0. Site mixing of Mn and Ni was allowed in the refinements and therefore it was possible to quantify the degree of ordering by evaluating the preferential occupation on the Ni-4a atomic site. It should be noted that 4a is the preferential Ni site while 12d is the preferential Mn site in the $P4_332$ structure. If Mn and Ni are randomly distributed over the 12d and 4a sites, the 4a occupancy would be 0.22 when the sample is fully disordered. Since the material is slightly Ni-deficient, the 4a occupancy can never reach full occupancy (i.e. 1) but the maximum possible ordering will show a Ni occupancy on this site of 0.88. With these limits in mind, the Ni-4a occupancy can be used to

quantify cation ordering in the samples. The changes in ordering with respect to temperature are shown in Figure 4(a). It is seen that a sharp increase in Ni-4a occupancy starts around 530˚C, and ordering continues to increase with temperature until 630˚C where disordering starts again. It is important to note that no oxygen release was observed until 725-730˚C when the same sample was tested with TGA. In order to ensure that the presence of isothermal steps has no significant effect in kinetic behaviour of oxygen release, a second TGA test (see Figure S3) with the same thermal history of the *in-situ* ND experiment was also performed. This test also confirms that no oxygen release is initiated in this temperature region. The cation disordering is thus not initiated by oxygen release.

After further heating, the sample temperature was kept constant during an isothermal step at 680˚C. At this temperature, cation ordering is mostly disrupted and the Ni-4a site occupancy becomes stable around 0.34. Following the isothermal step at 680 ˚C, the sample is cooled and cation ordering is quickly recovered. With increasing time during another isothermal step at 604˚C, the Ni-4a occupancy reaches 0.6, which corresponds to a 58% degree of ordering. These isothermal steps show that there is not a specific transition temperature separating completely ordered and disordered phases, but rather there is a temperature window for transition in which ordering degree gradually changes indicating a second-order transformation. This is similar to ordering transition observed in beta-brass (CuZn).[38] The archetypical ordering examples of first and second order transformations are Cu_3Au and CuZn, respectively. [39] In second-order transformations, ordering kinetics can be expected to be faster with an analogy to spinodal decomposition as compared to nucleation/growth observed in first-order transformations.[40] In the case of already ordered samples (cation mixing is already removed), Casas-Cabanas *et al.* reported that long annealing times are required to attain long-range order in LNMO crystals (via removal of anti-phase boundaries) with a similarity to ordering in Cu_3Au alloy.[28] It should be noted at this point that the evolution of cation ordering (removal of cation mixing) with temperature is discussed in this study and this process, particularly in the early stages, seems to proceed with relatively faster kinetics.

In the final heating/cooling step (note that the heating/cooling rate was doubled), ordering started to be disrupted around 640˚C and full disordering was achieved at temperatures around 730˚C. Since the ordering-disordering transition occurs over a temperature window and heating/cooling rate also affects this window, it is necessary to define a term that can be used for comparison purposes in future studies. In this study, T_{O-D} will refer to the temperature at which 50% ordering is achieved in case of very slow heating/cooling. This would obviously require very long measurement times, however, the average value of T_{O-D} during relatively faster cooling/heating can be used to estimate T_{O-D}. For 1˚C/min rate, 50% ordering is reached at 633-634˚C during heating and at 607-608˚C during cooling, which would give an average value of 620˚C for T_{O-D}. Similarly, for 2˚C/min rate, T_{O-D} is estimated as 617 ˚C which is in good agreement with the previous value considering the error bars in Figure 4(a).

These results show that oxygen release from LNMO has no direct role in driving the cation disordering, since disordering starts at significantly lower temperatures compared to the onset of oxygen release. This is an important observation as it shows us that it is possible to obtain samples with varying degrees of ordering without changing the oxygen content if suitable annealing temperature, gas environment and cooling rates are chosen during heat treatment. Secondly, when compared to work by Cai *et al.* which studied ordering for the stoichiometric LNMO compound (Mn:Ni ratio of 3:1),[15] our results show that the excess Mn in the chemical formula causes a decrease in T_{O-D} as most of the ordering is lost at 680˚C (no significant oxygen vacancy is expected at this temperature due to slow heating rate and prior isothermal step at 604˚C). The presence of Mn^{3+} seems to lower the tendency towards ordering to some degree, as also reported in earlier studies.[20,41] In the study by Kunduraci and Amatucci,[20] which was based on *ex-situ* analysis of quenched samples, it was suggested that the oxygen loss determines the ordering-disordering transition temperature. However, as demonstrated in this study, there is no direct relation between these two processes. On the other hand, oxygen loss can still cause disordering if certain conditions are not met. Theoretical calculations show that the energy difference between ordered and disordered phases can be significantly lowered by introduction of oxygen vacancies.[42] In other words, presence of oxygen vacancies would reduce the thermodynamical driving force for keeping the cation ordering at high temperature. When our findings are considered in context of previous studies, it can be

suggested that if T_{O-D} is slightly higher than the oxygen release temperature, then the formation of oxygen vacancies would spontaneously lower the measured T_{O-D} during heating to the same temperature as the onset of oxygen release. Introduction of Mn^{3+} due to oxygen release, either via oxygen vacancies or rock-salt phase formation, could also give such an effect as having excess Mn in the composition was shown to lower T_{O-D}. This would explain the coincidence of ordering-disordering and oxygen release temperature. However, even the oxygen release could affect T_{O-D}, they are not directly related. If the oxygen release temperature is made higher than T_{O-D} (e.g. by increasing oxygen partial pressure), cation disordering will begin independently from the onset of oxygen release as observed in our study.

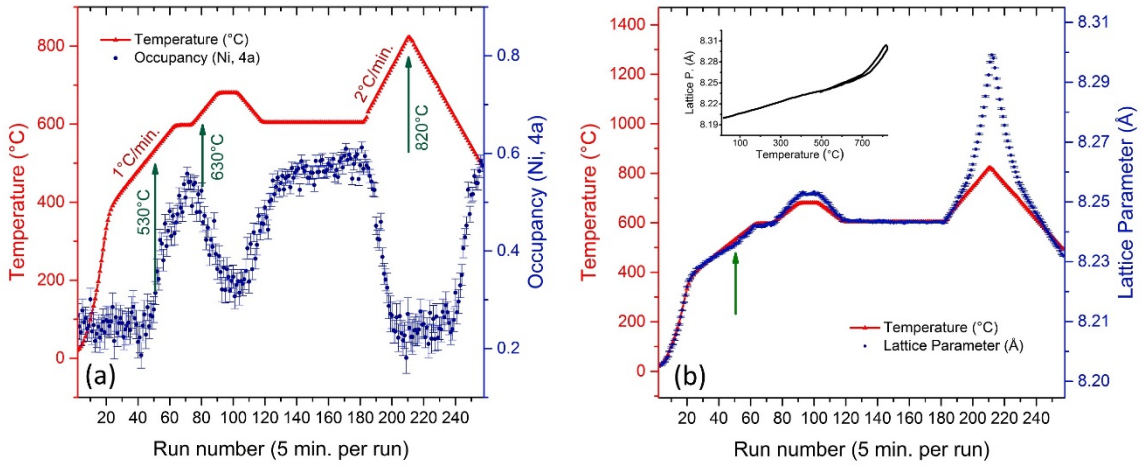

Figure 4. Change of Ni (4a) occupancy with temperature as obtained from sequential Rietveld refinements (a). Ni (4a) occupancy can be interpreted as the degree of cation ordering. Its value is 0.22 for fully disordered phase and 0.88 for the maximum ordering possible for the $LiNi_{0.44}Mn_{1.56}O_4$ sample. The change of lattice parameter with temperature is shown in (b). For easier evaluation, y-left and y-right axes are scaled so that the lines initially overlap completely (any disruption of the overlap is an indication of structural changes). A graph of lattice parameter vs. temperature is also shown as an inset (in high temperature region, lattice parameter is slightly higher during cooling as a result of kinetic limitations).

If oxygen vacancy formation is assumed to cause weight change alone (see Figure 1 for the TGA analysis), the corresponding change in occupancies would still be small in the temperature range studied here (e.g. 0.985 at 780˚C). Therefore, the oxygen occupancy was fixed to 1.0 for both oxygen sites (24e and 8c). While the oxygen content could not be directly analyzed from the ND data, an attempt was made to get information about the possible chemical changes by following the trends in lattice parameter with temperature. In Figure 4(b), these are presented by scaling the y-axes so that both lines initially overlap with each other. In this way, any deflections from linearity between the rate of lattice expansion and the temperature increase becomes clear. It is then seen that a deflection towards lower values starts around 460˚C, which corresponds to the temperature at which oxygen uptake also starts (see Figure 1). This is in accordance with the reduction in Mn^{3+} amount. The rate of cell parameter expansion starts to increase around 520˚C. This is in close proximity to the temperature at which cation ordering starts. Even though the variations are quite small, it indicates that the oxygen uptake during heating reduces the rate of lattice expansion, while the cation ordering increases it. Above 730˚C, a comparably larger increase in the rate of cell expansion occurs. This is in agreement with the considerable oxygen release expected at these temperatures. It is not possible to draw any direct conclusions by evaluating these trends. However, it was also observed that there was no rock-salt phase formed until 800˚C (and only negligible fractions at 820˚C). Therefore, it can be speculated that higher lattice constants are likely caused by oxygen vacancies. Nevertheless, possibility of rock-salt phase formation in very small amounts (in such a way that it is not detectable by diffraction) should not be completely ruled out. A slight increase in lattice constant also seems to originate from cation ordering, although more efficient packing could be expected for the ordered phase.

Characterization of LNMO samples used in LNMO-LTO full cells. In the first part of this study, it is shown that the disordering and oxygen release are not necessarily linked to each other. The conditions required to obtain LNMO powders with varying degrees of ordering while not changing the oxygen content (or to obtain disordered powders having varying oxygen content) have been described. This knowledge will lead to new studies focusing solely on the effect of disordering (or oxygen content) on the electrochemical performance. As part of this study, we heat treated LNMO powders to obtain conventionally named 'ordered' and 'disordered' samples. As mentioned earlier, the terms 'ordered' and 'disordered' are not well defined. In the majority of research papers, either of these phases is normally assigned to synthesized powders while the possibility of partial ordering is usually ignored. Additionally, even if the terms ordered and disordered are used, it is usually not the ordering alone, but also other related properties, e.g. oxygen deficiency and Mn^{3+} content, which possibly affect the electrochemical performance. Therefore, in the second part of this study, 'ordered' and 'disordered' samples were carefully characterized with respect to their oxygen content and their ordering degree. Following this, their electrochemical performance was tested in full cells in order to have a reference point to compare to previous literature. 'Ordered' samples were obtained by annealing starting powders at 600˚C (for 12 hours) which were thereafter cooled slowly (all performed under oxygen flow). In order to obtain 'disordered' samples, powders were annealed at 800˚C (under air) for the same duration and later quenched to room temperature. Starting powders were also characterized and will be referred as 'reference' through the rest of the article.

Neutron diffraction (ND) patterns together with the calculated models (via Rietveld refinements) are shown in Figure 5. The ordered sample shows intense superlattice peaks indicating a high degree of cation ordering in the structure (see Figure 5a). As obtained from Rietveld refinements, the Ni-4a occupancy is ~ 0.8. If a maximum possible occupancy of Ni-4a (0.88) is taken as 100% and minimum (0.22) as 0%, the degree of ordering can be represented as ~87% for the 'ordered' sample. The ND pattern for the reference sample is shown in Figure 5(b). At first sight, no superlattice peaks are observable which indicates the presence of a fully disordered structure. However, when inspected carefully, it is possible to see the presence of weak, very broad, overlapping peaks at positions where superlattice reflections are expected. Therefore, during the refinements, cation mixing was allowed and as a result Ni-4a was found to be ~ 0.45. This would correspond to an ordering degree of ~ 35%, which could be considered a 'partial ordering'. Ordered domains might be homogeneously distributed through the particles, or be concentrated near the surface or the core. At the onset of ordering, it is reasonable to expect the same orientation for the new ordered domains with respect to the host crystals. Therefore, while the superlattice peaks are broadened due to size effects, such broadening would not be expected for the sublattice peaks, thus causing anisotropic broadening. A separate refinement of peak broadening for superlattice peaks are possible with other softwares.[18,28] Due to anisotropic broadening, the fit was worse in regions where superlattice peaks are expected. Therefore, some degree of error should be considered for this specific sample (the real Ni-4a occupancy value would be slightly higher than the calculated number, i.e. 0.45).

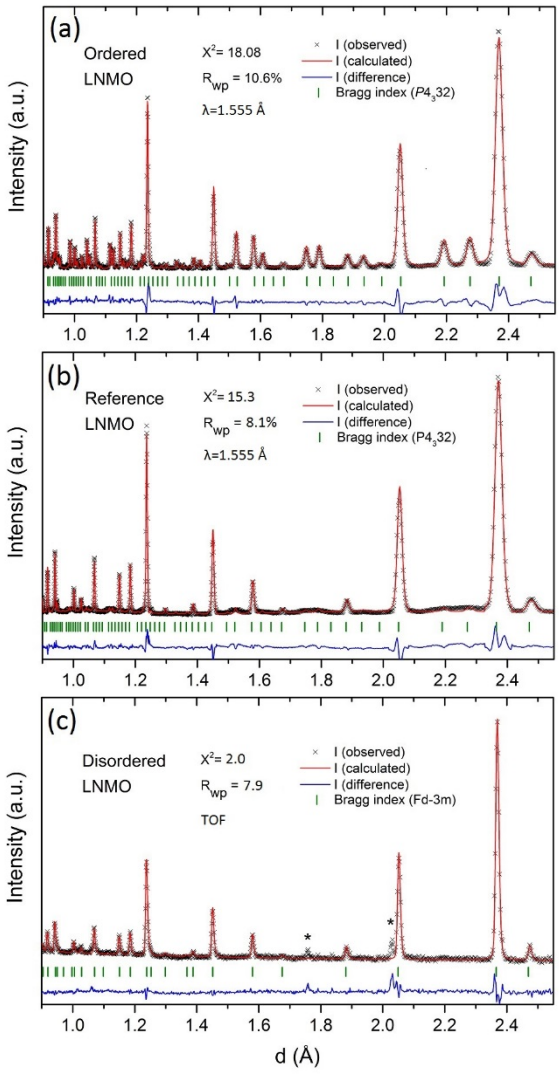

Figure 5. Neutron diffraction patterns (at room temperature) with calculated patterns from Rietveld refinements of ordered sample (a), reference sample (b) and disordered sample (c). The ordered and reference samples were measured using a 'constant wavelength' diffractometer while the disordered sample was measured on a different 'TOF' diffractometer. Peaks marked with * are due collimating mask.

In the case of the disordered sample, no trace of superlattice peaks was visible. This pattern also corresponds to the initial data (prior to heating) in the *in-situ* diffraction experiment, which gave a Ni-4a value of 0.22 (0% ordering) when modelled using the $P4_332$ symmetry. Therefore, refinement here was made using the *Fd*-3*m* structure. Structural parameters obtained from the refinements are provided in Table 1 for all three samples. Based on these refinement results, the three samples can be categorized as 'highly ordered', 'partially ordered' and 'fully disordered' LNMO samples.

Table 1. Structural parameters (at room temperature) obtained from Rietveld refinements for ordered, reference and disordered samples (U_{iso} parameters were refined alone after the initial refinement of positions and occupancies and in later stages of refinements U_{iso} parameters were fixed).

Wyckoff position	X	Y	Z	Occupancy	U_{iso} (Å^2)
Ordered sample					
Li – 8c	0.0016(13)	0.0016(13)	0.0016(13)	1	0.015
Mn – 4a	0.625	0.625	0.625	0.204(4)	0.006
Ni – 4a	0.625	0.625	0.625	0.796(4)	0.006
Mn – 12d	0.125	0.3794(7)	-0.1294(7)	0.972(1)	0.006
Ni – 12d	0.125	0.3794(7)	-0.1294(7)	0.028(1)	0.006
O – 8c	0.3861(3)	0.3861(3)	0.3861(3)	1	0.004
O – 24e	0.1475(3)	-0.1417(2)	0.1263(3)	1	0.007
***P4$_3$32, a=b=c=8.1947(1),*** *χ2 = 18.08, Rp = 8.3%, wRp = 10.56%.*					
Reference sample					
Li – 8c	0.0025(20)	0.0025(20)	0.0025(20)	1	0.013
Mn – 4a	0.625	0.625	0.625	0.551(5)	0.006
Ni – 4a	0.625	0.625	0.625	0.449(5)	0.006
Mn – 12d	0.125	0.3806(23)	-0.1306(23)	0.856(2)	0.006
Ni – 12d	0.125	0.3806(23)	-0.1306(23)	0.144(2)	0.006
O – 8c	0.3875(3)	0.3875(3)	0.3875(3)	1	0.003
O – 24e	0.1415(4)	-0.1376(4)	0.1249(3)	1	0.011
***P4$_3$32, a=b=c=8.2023(1),*** *χ2 = 15.29, Rp = 6.1%, wRp = 8.1%.*					
Disordered sample					
Li – 8a	0.375	0.375	0.375	1	0.013
Mn – 16d	0	0	0	0.78	0.004
Ni – 16d	0	0	0	0.22	0.004
O – 32e	0.2368(0)	0.2368(0)	0.2368(0)	1	0.020
Fd-3m, a=b=c=8.2001(2), *χ2 = 2.01, Rp = 7.93%, wRp = 7.36%.*					

Following the characterization of cation ordering, the oxygen deficiency in the samples was also determined using TGA analysis. For this purpose, all samples were heated and cooled under pure oxygen flow (see Figure 6a). There is slight oxygen deficiency for the reference when compared to the highly ordered sample. In contrast, the difference is significantly higher for the fully disordered sample. This behaviour can be explained by the observations made in the first part since the cation ordering is not necessarily connected with the amount of oxygen content.

While a precise determination of cation ordering is possible with neutron diffraction, this technique's availability to most researchers is limited and often some other analytical tools are used to make qualitative comparison between ordered and disordered samples. One of these techniques is Raman spectroscopy, which is sensitive to atom vibrations and crystal symmetries, and is comparatively more available than neutron diffraction. In Figure 6(b), we show characteristic Raman spectra for the samples previously investigated by neutron diffraction (ND). For comparison purposes, it should be reminded that neutron diffraction probes the whole sample depth while Raman spectroscopy is relatively surface sensitive (typical probing depths of 20-300 nm)[43] and LNMO powders used in this work are micron-scaled. As seen in Figure 6(b), the two most obvious differences are observed for peaks located at 162 and 407 cm^{-1}. These are assigned to Ni-O bands and their intensity increases with the degree of ordering.[16,44] The spectrum of the ordered LNMO sample displays sharper peaks and also three minor features approximately around 218 cm^{-1}, 240 cm^{-1} and 328 cm^{-1}, together with an evident peak splitting at 594 and 613 cm^{-1} for one of the Mn-O vibrations, matching well with earlier observations.[45] All together, these characteristic peaks for the ordered specimen suggest the formation of a superlattice[45]

and the sharpness of its Raman bands can be related with well-separated Ni and Mn sites. In fact, the splitting between the peaks around 594 and 613 cm^{-1} disappears with increasing disorder, yielding only a broad band in agreement with previous studies.[4] The intensities of the most intense peaks around 496 cm^{-1} and 638 cm^{-1} are also changed in disordered and ordered samples, in line with previous reports.[45] The observations made for the reference sample is qualitatively comparable to the neutron diffraction results and indicates that partial ordering is not solely concentrated near the surface or the core of micron-scaled samples (since otherwise Raman spectra for the reference sample would be similar to ordered sample, or disordered sample, respectively).

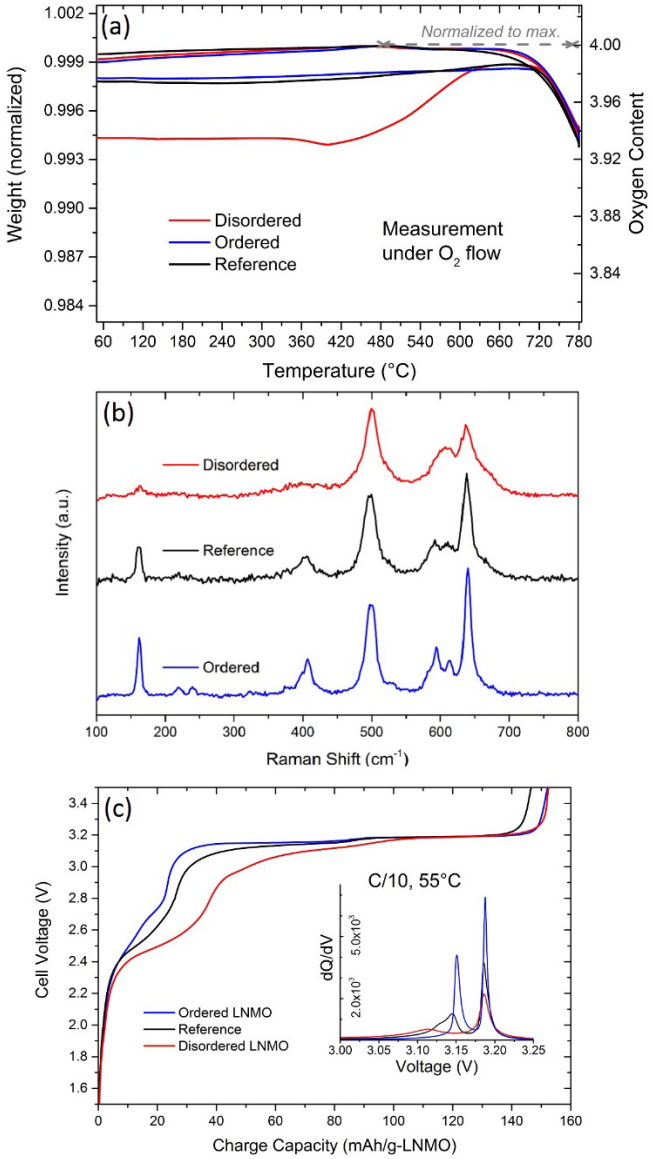

Figure 6. Comparison of the amount of oxygen uptake for ordered, reference and disordered LNMO during heating/cooling under oxygen as obtained from TGA analysis (a). The right y-axis here is given with the assumption of only oxygen vacancy formation. In (b), normalized Raman spectra for the same samples are shown. In (c), first voltage curves for the three samples are shown while the inset shows differential charge change with respect to voltage for the high voltage region.

As a final complementary analysis, we also looked at voltage curves during the first charge, as the shape of the curve would depend both on cation ordering and oxygen deficiency. The results are shown in Figure 6(c). Here the curves were obtained from LNMO-LTO full cells (note that LTO has a flat voltage plateau around 1.55 V vs. Li^+/Li). The main differences are observed in the low voltage region (2.2-3.0

V) where mostly Mn^{3+}/Mn^{4+} activity is expected. While the behavior of the highly ordered and reference samples are relatively similar, it is significantly different for the disordered sample. This is in accordance with the trends observed for oxygen recovery (see Figure 6a). This is not surprising since oxygen loss would introduce Mn^{3+} into the structure. While highly ordered and reference samples were relatively similar, some differences were still distinct. Highly ordered samples had relatively higher voltage in this region (2.2-3.0 V) and the plateau had two characteristic shoulders. Splitting of this region into two shoulders, related to ordering, was reported for Mn-rich samples in previous studies.[8,20]

The inset in Figure 6(c) shows a zoomed-in view of the 3.0-3.25 V region, and for an easier interpretation it is represented as 'dQ/dV vs. V' in 'y' and 'x' axes, respectively. There are two high voltage peaks in this region. The first one has a sharp peak (i.e. flat plateau) at 3.15 V for the ordered sample while it becomes gradually broadened (i.e. more sloped in the voltage profile) in the reference (~ 3.14 V) and disordered samples (~ 3.11 V). The second plateau is observed at 3.19 V for all samples and the main differences occur through peak widths (increase with disordering). During charging, as the Li is extracted from tetrahedral sites, it would leave vacant Li sites (VLi). It was reported that a configuration with *Li–VLi–Li–VLi* would be energetically favored rather than *Li–Li* or *VLi–VLi* pairs, especially at Li– occupancy (x) = 0.5.[46] It was also suggested that cation disordering is compatible with such favorable *Li–VLi* configurations for $x > 0.5$, and accordingly a voltage step near $x = 0.5$ is observed for disordered samples.[46] In agreement with this explanation, the peak at 3.19 V ($x < 0.5$) does not move while the second peak ($x > 0.5$) shifts to lower values with decreasing cation ordering.

Electrochemical characterization in LNMO-LTO full cells. Following the *in-situ* and *ex-situ* characterization of LNMO samples, testing of electrochemical performance was performed. It is known that cyclable lithium loss can play a significant role in the fading of LNMO based cells, however, this type of contribution is only observable in full cells, since there is practically unlimited Li reserves in the Li electrode in half cells. Additionally, Li electrodes in half cells can contribute significantly to internal cell resistance, especially during high rate cycling. Therefore, LTO was used as negative electrode due to its good electrochemical stability and rate capability. It was shown in our previous paper that the electrochemical cross-talk, i.e. migration of oxidized products, dissolved metal ions, etc. from LNMO to LTO is the main reason of capacity fading.[33] If the samples characterized in the previous section (e.g. highly ordered, partially ordered and fully disordered) have a different tendency towards electrolyte oxidation and transition metal dissolution, this would also be reflected in capacity during cycling of LNMO-LTO cells. In the same study,[33] it was shown that LTO had limited contribution to cell resistance during cycling. Therefore, it is possible to evaluate rate capability of different LNMO samples in such a full cell chemistry. Since performance degradation of LNMO-based cells is accelerated at elevated temperature, we performed all cell testing at 55˚C.

In Figure 7, galvanostatic cycling results of full cells cycled at C/10 rate are shown. It is seen that differences in capacity and coulombic efficiency are small and are likely within the reproducibility error of the tested cells. This indicates that the degree of side reactions are similar for all three samples. After 30 cycles, degradation of the highly ordered sample is accelerated (roll-over point) while a similar behaviour is observed for the reference sample (partially ordered) after 40 cycles. It is likely that the disordered sample would also reach such a roll-over point if the cycling was to be continued. As seen from the selected voltage curves in Figure 7(b-d), there is a gradual increase in overpotential with increasing cycling number, and this increase is more severe for the ordered and reference sample. It is also seen from voltage curves that the differences in observed capacity fading is dominated by kinetic limitations evolving during cycling, rather than the differences in cyclable lithium loss, which is in agreement with the similar coulombic efficiency values.

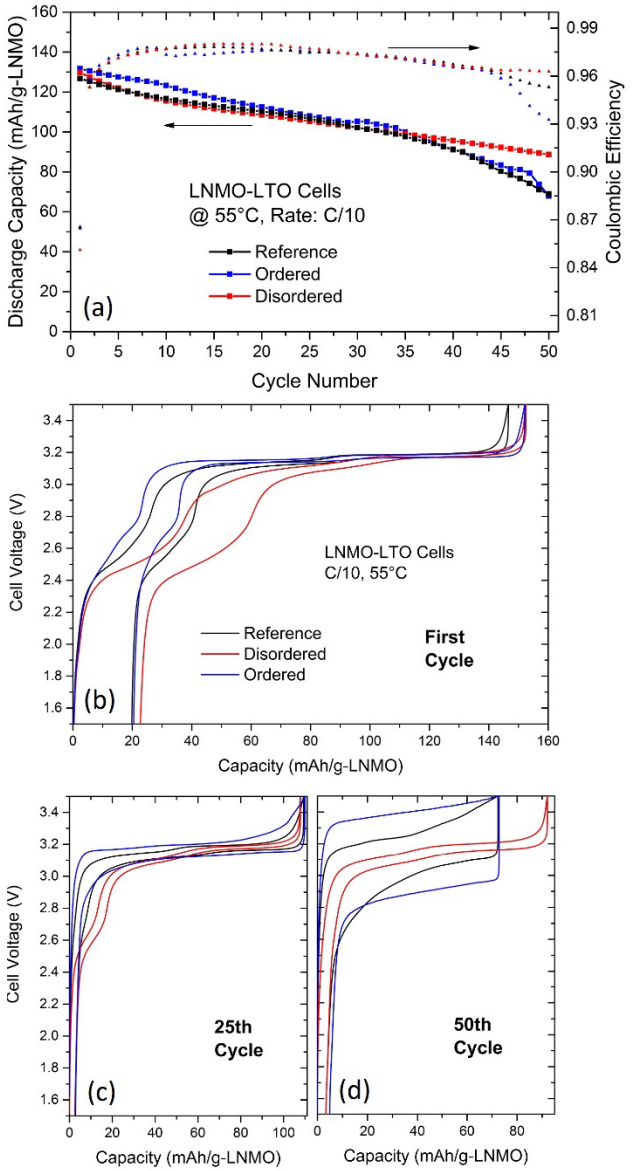

Figure 7. Galvanostatic cycling of LNMO-limited LNMO-LTO full cells at 55˚C and C/10 rate (a). Selected voltage curves are shown in (b) for the first cycle, in (c) for the 25th and (d) for the 50th cycle.

A second set of full cells have also been tested at 1C rate (Figure 8a). The initial performances of all three samples are comparable, nevertheless a relatively better capacity retention is seen for the disordered sample. As expected for 1C cycling rate, more drastic roll-over points are observed when compared to C/10 cycling (Figure 7). First, the highly ordered sample fails, which is followed by the reference and disordered sample, respectively. These observations indicate that the rate capabilities are similar for all three samples initially, but that these change during cycling. It is common to attribute the better performance of the disordered samples to enhanced electronic[3] and ionic conductivity.[47] More recent studies show that the electronic conductivities are comparable when the whole lithiation range is considered.[4,25] Similar values of ionic conductivity have also been reported.[4] In agreement with these results, our observations also do not indicate any significant differences in intrinsic rate capability of samples. On the other hand, after some duration of cycling, disordering (or oxygen deficiency) clearly improves the retention of initial rate capability. If this capacity difference originates primarily from structural degradation related to volume change and strain during charging–discharging, the fading rate would be expected to be more dependent on 'cycle number' than on 'cycling time'. Comparison of Figure 7 (C/10 rate) and Figure 8 (1C) show that the fading of cells is more dependent on 'time' rather than on 'cycle number' which is usually the case when parasitic reactions cause the cell degradation.[48]

However, similar coulombic efficiency and cyclable lithium loss of cells indicate that the differences are not caused simply by the varying tendency of samples towards electrolyte oxidation on the surface.

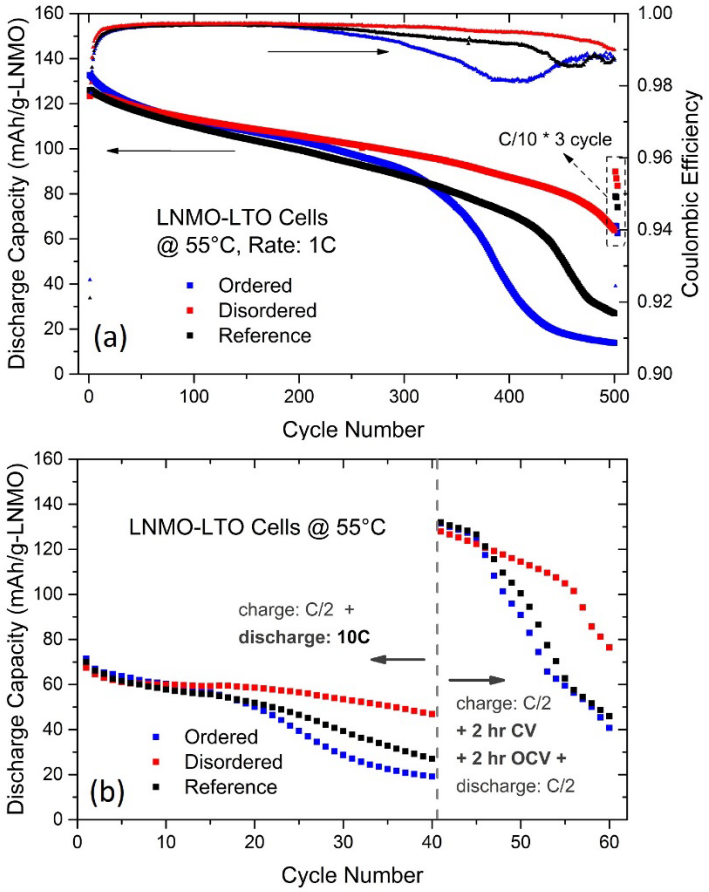

Figure 8. Galvanostatic cycling results of LNMO-limited LNMO-LTO full cells at 55˚C and 1C rate (a). In (b), similar cells were initially cycled asymmetrically (C/2 for charging and 10C for discharging) and later were cycled at C/2 rate symmetrically, however, there was a 2 hour constant voltage step (3.5 V) and a 2 hour OCV step at the fully charged state to make cycling conditions more severe in terms of side reactions on LNMO.

In order to obtain more information on cell degradation, we performed a combined cell testing procedure (see Figure 8b) with an aim to test both intrinsic rate capability and high voltage stability for the same cells. Despite the fact that initial performances were similar in Figure 8 (a), intrinsic rate capability can still play a role in performance degradation. This can be due to slightly higher overpotentials caused by ordering, especially in the 3.0–3.2 V region. As a possibility, such an overpotential during charging can accelerate the issues related to high voltage instability and subsequent reduction of power performance. Therefore, in the first part of cycling, the charging rate was set to C/2 to minimize any effects coming from differences in the overpotential. In contrast to charging, the electrodes are less prone to side reactions during discharge. We therefore tested rate capability on discharge and applied a 10C rate so that any difference due to intrinsic rate capability would be easier to observe. In Figure 8(b), for nearly 15 cycles all cells behave similarly even at a high rate of 10C. Changes instead only evolve afterwards. In the second part of testing, the charging rate was again C/2, however, this was followed by a constant voltage step at 3.5 V for a duration of two hours, and a subsequent OCV time-step (two hours). These steps were added to ensure ‘similarly severe’ conditions for all samples in terms of high voltage stability. Thus, any possible effect of overpotential would be eliminated. As the results demonstrate, adding those steps accelerate cell fading dramatically even at C/2 rate. The results in Figure 8(b) confirm that the rate capability of electrodes are almost the same initially, even at 10C discharging rate. Therefore, the different electrochemical performances are not likely caused by intrinsic rate capabilities but mainly originate from the changes occurring during cycling, which is seen to be more time dependent,

particularly for time when the batteries are in the high voltage region (i.e. low lithiation states). This further supports that the presence of Mn^{3+} does not play a significant role in performance through ionic/electronic conductivity or Mn dissolution tendency (via disproportionation reaction) as all Mn^{3+} are already consumed in low lithiation states.

Conclusions

In this study, the cation ordering–disordering transition in slightly Mn-rich LNMO has been studied during heating and cooling under pure oxygen atmosphere. As expected, TGA analysis confirms that the oxygen release from LNMO is shifted to higher temperatures (725-730 ˚C) when samples are heated under pure oxygen instead of air. However, cation ordering–disordering transition temperature (T_{O-D}) does not shift accordingly and the transition to disordering begins earlier, at 630˚C. Therefore, the disordering occurs in a temperature region where oxygen release is not observed, and it can be concluded that there is not a direct relation between oxygen release and (T_{O-D}), as suggested earlier.[20] It is also observed that the order to disorder transition takes place within a temperature window as opposed to a full transition at a particular temperature.

There is theoretical evidence that cation disordering would favor single-phase delithiation reactions, enabling access to solid-solution reaction paths, which is expected to be beneficial for electrochemical performance.[27] If it is only the disordering that improves the performance, but not the oxygen loss during sample preparation (e.g. Mn^{3+} presence and oxygen deficiency), then the minimization of oxygen loss while still maximizing the disordering would be desired for this material. Our *in-situ* ND experiment shows that it is indeed possible to tune disordering without causing oxygen deficiency nor rock-salt impurity phases, since no direct relation between oxygen release and T_{O-D} was found. As a recommendation for future studies, samples can be heated to a temperature which is in a range above T_{O-D} but below oxygen release temperature, and then quenched to room temperature to obtain disordered LMNO without causing oxygen loss. On the other hand, if the oxygen loss is the reason for the improved performance, then samples with optimum oxygen content will be desired. In this case, disordered samples having varying oxygen content can be obtained by annealing at different temperatures above T_{O-D} and the oxygen release temperature, but below rock-salt phase formation temperature, followed by quenching to room temperature.

In the second part of this study, LNMO powders were heat treated to obtain ‘ordered’ and ‘disordered’ samples as could be categorized in the literature and samples were quantitatively characterized together with the starting powders to determine their relative oxygen content and cation ordering. Electrochemical testing in full cells showed that even at 10C discharge rate (at 55˚C), initial performances of all three samples are nearly identical. This observation contradicts the generally accepted explanation that disordered LNMO has a better intrinsic rate capability, while being in agreement with some recent publications[4,25] which suggest no significant difference in electronic and ionic conductivity of ordered and disordered samples. However, as the cycling proceeds, fast degradation of rate capability was observed for highly ordered samples while the retention was better for disordered samples. If the degradation was mainly originated from subsequent phase changes and expansion/shrinkage during cycling, dependency on cycle number would be expected. Surprisingly, this degradation is rather dependent on time than on number of cycles, and this indicates that the reasons behind the degradation are more related to instability of LNMO at higher voltages – i.e., at lower lithiation states. Even though similar coulombic efficiencies were observed for all samples, the differences in electrochemical performance might still originate from variances in reaction products (e.g. products causing pore clogging)[33] or near surface structural changes such as formation of reconstruction layers (e.g. rock-salt surface layers)[49–51] or transition metal dissolution,[52,53] etc. Future work should be performed to determine if it is the disordering or oxygen content that dominates the differences in electrochemical performance. It is seen that conventionally prepared samples are not ideal for this purpose. In light of these findings, we suggest that upcoming studies should focus on the performance comparison of LNMO samples that have varying amount of ordering but having the same oxygen

content (and also of equally disordered samples having varying amount of oxygen content). Our findings from the first of part of this study will guide such future studies.

Acknowledgement

We thank the UK Science and Technology Facilities Council (STFC) for provision of neutron diffraction beam time at the ISIS Neutron and Muon Source. Institute for Energy Technology, Norway, is also acknowledged for the neutron diffraction analysis of samples in powder neutron diffractometer PUS in the JEEP II reactor. Henrik Eriksson is acknowledged for his support for the TGA instrument. Leclanché are also gratefully acknowledged for providing the LTO electrodes. We are also thankful to Dr. Edyta Nagrodzka for the ICP-OES measurement. Volkswagen AG and Scania CV AB are acknowledged for the financial support. The authors also acknowledge support from the Swedish Energy Agency (project no. 42031-1) and StandUp for Energy.

Supporting Information

S1. Selected patterns (2.02-2.45Å) from the *in-situ* neutron diffraction experiment. S2. Single neutron diffraction data of run number 210 from the *in-situ* neutron diffraction experiment. S3. TGA test results of disordered LNMO under oxygen flow with an identical thermal history of *in-situ* neutron diffraction experiment.

References

(1) Julien, C. M.; Mauger, A. Review of 5-V Electrodes for Li-Ion Batteries: Status and Trends. *Ionics (Kiel).* **2013**, *19*, 951–988. https://doi.org/10.1007/s11581-013-0913-2.

(2) Manthiram, A.; Chemelewski, K.; Lee, E.-S. A Perspective on the High-Voltage LiMn1.5Ni0.5O4 Spinel Cathode for Lithium-Ion Batteries. *Energy Environ. Sci.* **2014**, *7*, 1339. https://doi.org/10.1039/c3ee42981d.

(3) Kunduraci, M.; Al-Sharab, J. F.; Amatucci., G. G. High-Power Nanostructured LiMn2-XNixO4 High-Voltage Lithium-Ion Battery Electrode Materials: *Chem. Mater* **2006**, *18*, 3585–3592. https://doi.org/10.1021/cm060729s.

(4) Amin, R.; Belharouk, I. Part I: Electronic and Ionic Transport Properties of the Ordered and Disordered LiNi 0.5 Mn 1.5 O 4 Spinel Cathode. *J. Power Sources* **2017**, *348*, 311–317. https://doi.org/10.1016/j.jpowsour.2017.02.071.

(5) Kim, J. H.; Pieczonka, N. P. W.; Li, Z.; Wu, Y.; Harris, S.; Powell, B. R. Understanding the Capacity Fading Mechanism in LiNi0.5Mn 1.5O4/Graphite Li-Ion Batteries. *Electrochim. Acta* **2013**, *90*, 556–562. https://doi.org/10.1016/j.electacta.2012.12.069.

(6) Wang, L.; Li, H.; Huang, X.; Baudrin, E. A Comparative Study of Fd-3m and P4332 "LiNi0.5Mn1.5O4." *Solid State Ionics* **2011**, *193*, 32–38. https://doi.org/10.1016/j.ssi.2011.04.007.

(7) Kim, J.-H.; Myung, S.-T.; Yoon, C. S.; Kang, S. G.; Sun, Y.-K. Comparative Study of LiNi0.5Mn1.5O4-δ and LiNi0.5Mn1.5O4 Cathodes Having Two Crystallographic Structures: Fd $\bar{3}$m and P 4332. *Chem. Mater.* **2004**, *16*, 906–914. https://doi.org/10.1021/cm035050s.

(8) Song, J.; Shin, D. W.; Lu, Y.; Amos, C. D.; Manthiram, A.; Goodenough, J. B. Role of Oxygen Vacancies on the Performance of LiNi0.5-XMn 1.5+xO 4 (x = 0, 0.05, and 0.08) Spinel Cathodes for Lithium-Ion Batteries. *Chem. Mater.* **2012**, *24*, 3101–3109. https://doi.org/10.1021/cm301825h.

(9) Zheng, J.; Xiao, J.; Yu, X.; Kovarik, L.; Gu, M.; Omenya, F.; Chen, X.; Yang, X.-Q.; Liu, J.; Graff, G. L.; et al. Enhanced Li+ Ion Transport in LiNi0.5Mn1.5O4 through Control of Site Disorder. *Phys. Chem. Chem. Phys.* **2012**, *14*, 13515. https://doi.org/10.1039/c2cp43007j.

(10) Cabana, J.; Casas-Cabanas, M.; Omenya, F. O.; Chernova, N. A.; Zeng, D.; Whittingham, M. S.; Grey, C. P. Composition-Structure Relationships in the Li-Ion Battery Electrode Material LiNi 0.5 Mn 1.5 O 4. *Chem. Mater.* **2012**, *24*, 2952–2964. https://doi.org/10.1021/cm301148d.

(11) Chemelewski, K. R.; Lee, E. S.; Li, W.; Manthiram, A. Factors Influencing the Electrochemical Properties of High-Voltage Spinel Cathodes: Relative Impact of Morphology and Cation Ordering. *Chem. Mater.* **2013**, *25*, 2890–2897. https://doi.org/10.1021/cm401496k.

(12) Kunduraci, M.; Amatucci, G. G. The Effect of Particle Size and Morphology on the Rate Capability of 4.7 V LiMn1.5Ni0.5O4 Spinel Lithium-Ion Battery Cathodes. *Electrochim. Acta* **2008**, *53*, 4193–4199. https://doi.org/10.1016/j.electacta.2007.12.057.

(13) Li, W.; Song, B.; Manthiram, A. High-Voltage Positive Electrode Materials for Lithium-Ion Batteries. *Chem. Soc. Rev.* **2017**, *46*, 3006–3059. https://doi.org/10.1039/C6CS00875E.

(14) Liu, G. Q.; Wen, L.; Liu, Y. M. Spinel LiNi0.5Mn1.5O4 and Its Derivatives as Cathodes for High-Voltage Li-Ion Batteries. *J. Solid State Electrochem.* **2010**, *14*, 2191–2202. https://doi.org/10.1007/s10008-010-1061-5.

(15) Cai, L.; Liu, Z.; An, K.; Liang, C. Unraveling Structural Evolution of LiNi0.5Mn1.5O4 by in Situ Neutron Diffraction. *J. Mater. Chem. A* **2013**, *1*, 6908. https://doi.org/10.1039/c3ta00145h.

(16) Kunduraci, M.; Amatucci, G. G. Synthesis and Characterization of Nanostructured 4.7 V LixMn1.5Ni0.5O4 Spinels for High-Power Lithium-Ion Batteries. *J. Electrochem. Soc.* **2006**, *153*, A1345. https://doi.org/10.1149/1.2198110.

(17) Duncan, H.; Hai, B.; Leskes, M.; Grey, C. P.; Chen, G. Relationships between Mn 3+ Content, Structural Ordering, Phase Transformation, and Kinetic Properties in LiNi x Mn 2– x O 4 Cathode Materials. *Chem. Mater.* **2014**, *26*, 5374–5382. https://doi.org/10.1021/cm502607v.

(18) Kim, J. H.; Huq, A.; Chi, M.; Pieczonka, N. P. W.; Lee, E.; Bridges, C. A.; Tessema, M. M.; Manthiram, A.; Persson, K. A.; Powell, B. R. Integrated Nano-Domains of Disordered and Ordered Spinel Phases in LiNi0.5Mn1.5O4 for Li-Ion Batteries. *Chem. Mater.* **2014**, *26*, 4377–4386. https://doi.org/10.1021/cm501203r.

(19) Chen, Y.; Cheng, Y.; Li, J.; Feygenson, M.; Heller, W. T.; Liang, C.; An, K. Lattice-Cell Orientation Disorder in Complex Spinel Oxides. *Adv. Energy Mater.* **2017**, *7*. https://doi.org/10.1002/aenm.201601950.

(20) Kunduraci, M.; Amatucci, G. G. Effect of Oxygen Non-Stoichiometry and Temperature on Cation Ordering in LiMn2-XNixO4 Spinels. *J. Power Sources* **2007**, *165*, 359–367. https://doi.org/10.1016/j.jpowsour.2006.11.051.

(21) Pasero, D.; Reeves, N.; Pralong, V.; West, A. R. Oxygen Nonstoichiometry and Phase Transitions in LiMn 1.5Ni0.5O4−δ. *J. Electrochem. Soc.* **2008**, *155*, A282. https://doi.org/10.1149/1.2832650.

(22) Zhong, Q.; Bonakclarpour, A.; Zhang, M.; Gao, Y.; Dahn, J. R. Synthesis and Electrochemistry of LiNiMn2 _ O4. *J Electrochem Soc* **1997**, *144*, 205–213. https://doi.org/10.1149/1.1837386.

(23) Shaju, K. M.; Bruce, P. G. Nano-LiNi0.5Mn1.5O4 Spinel: A High Power Electrode for Li-Ion Batteries. *Dalt. Trans.* **2008**, No. 40, 5471. https://doi.org/10.1039/b806662k.

(24) Bhandari, A.; Bhattacharya, J. Review—Manganese Dissolution from Spinel Cathode: Few Unanswered Questions. *J. Electrochem. Soc.* **2017**, *164*, A106–A127. https://doi.org/10.1149/2.0101614jes.

(25) Moorhead-Rosenberg, Z.; Huq, A.; Goodenough, J. B.; Manthiram, A. Electronic and Electrochemical Properties of Li1-XMn1.5Ni0.5O4 Spinel Cathodes As a Function of Lithium Content and Cation Ordering. *Chem. Mater.* **2015**, *27*, 6934–6945. https://doi.org/10.1021/acs.chemmater.5b01356.

(26) Samarasingha, P. B.; Sottmann, J.; Margadonna, S.; Emerich, H.; Nilsen, O.; Fjellvåg, H. In Situ Synchrotron Study of Ordered and Disordered LiMn 1.5 Ni 0.5 O 4 as Lithium Ion Battery Positive Electrode. *Acta Mater.* **2016**, *116*, 290–297. https://doi.org/10.1016/j.actamat.2016.06.040.

(27) Lee, E.; Persson, K. A. Solid-Solution Li Intercalation as a Function of Cation Order/Disorder in the High-Voltage LixNi0.5Mn1.5O4 Spinel. *Chem. Mater.* **2013**, *25*, 2885–2889. https://doi.org/10.1021/cm4014738.

(28) Casas-Cabanas, M.; Kim, C.; Rodríguez-Carvajal, J.; Cabana, J. Atomic Defects during Ordering Transitions in $LiNi_{0.5}Mn_{1.5}O_4$ and Their Relationship with Electrochemical Properties. *J. Mater. Chem. A* **2016**, *4*, 8255–8262. https://doi.org/10.1039/C6TA00424E.

(29) Chen, Y.; Sun, Y.; Huang, X. Origin of the Ni/Mn Ordering in High-Voltage Spinel LiNi0.5Mn1.5O4: The Role of Oxygen Vacancies and Cation Doping. *Comput. Mater. Sci.* **2016**, *115*, 109–116. https://doi.org/10.1016/j.commatsci.2016.01.005.

(30) Vitucci, F. M.; Paolone, A.; Palumbo, O.; Greco, G.; Lombardo, L.; K??ntje, M.; Latini, A.; Panero, S.; Brutti, S. High-Temperature Structural Evolution of the Disordered LiMn1.5Ni0.5O4. *J. Am. Ceram. Soc.* **2016**, *99*, 1815–1822. https://doi.org/10.1111/jace.14166.

(31) Samarasingha, P. B.; Andersen, N. H.; Sørby, M. H.; Kumar, S.; Nilsen, O.; Fjellvåg, H. Neutron Diffraction and Raman Analysis of LiMn1.5Ni0.5O4 Spinel Type Oxides for Use as Lithium Ion Battery Cathode and Their Capacity Enhancements. *Solid State Ionics* **2016**, *284*, 28–36. https://doi.org/10.1016/j.ssi.2015.11.018.

(32) Zhao, B.; Ran, R.; Liu, M.; Shao, Z. A Comprehensive Review of Li4Ti5O12-Based Electrodes for Lithium-Ion Batteries: The Latest Advancements and Future Perspectives. *Mater. Sci. Eng. R Reports* **2015**, *98*, 1–71. https://doi.org/10.1016/j.mser.2015.10.001.

(33) Aktekin, B.; Lacey, M. J.; Nordh, T.; Younesi, R.; Tengstedt, C.; Zipprich, W.; Brandell, D.; Edström, K. Understanding the Capacity Loss in LiNi 0.5 Mn 1.5 O 4 –Li 4 Ti 5 O 12 Lithium-Ion Cells at Ambient and Elevated Temperatures. *J. Phys. Chem. C* **2018**, *122*, 11234–11248. https://doi.org/10.1021/acs.jpcc.8b02204.

(34) Hull, S.; Smith, R. I.; David, W. I. F.; Hannon, A. C.; Mayers, J.; Cywinski, R. The Polaris Powder Diffractometer at ISIS. *Phys. B Phys. Condens. Matter* **1992**, *180–181*, 1000–1002. https://doi.org/10.1016/0921-4526(92)90533-X.

(35) Larson, A. C.; Von Dreele, R. B. General Structure Analysis System (GSAS). *Los Alamos Natl. Lab. Rep. LAUR 86-748* **2004**.

(36) Toby, B. H. EXPGUI, a Graphical User Interface for GSAS. *J. Appl. Crystallogr.* **2001**, *34*, 210–213. https://doi.org/10.1107/S0021889801002242.

(37) Hauback, B. C.; Fjellvåg, H.; Steinsvoll, O.; Johansson, K.; Buset, O. T.; Jørgensen, J. The High Resolution Powder Neutron Diffractometer PUS at the JEEP II Reactor at Kjeller in Norway. *J. Neutron Res.* **2000**, *8*, 215–232. https://doi.org/10.1080/10238160008200055.

(38) Als-Nielsen, J.; Dietrich, O. W. Long-Range Order and Critical Scattering of Neutrons below the Transition Temperature in β-Brass. *Phys. Rev.* **1967**, *153*, 717–721. https://doi.org/10.1103/PhysRev.153.717.

(39) Keating, D. T.; Warren, B. E. Long-Range Order in Beta-Brass and Cu 3 Au. *J. Appl. Phys.* **1951**, *22*, 286–290. https://doi.org/10.1063/1.1699944.

(40) Porter, D., Easterling, K., Sherif, M. Y. *Phase Transformations in Metals and Alloys, Third Edition (Revised Reprint)*; CRC Press, 2009. https://doi.org/10.1201/9781439883570.

(41) Xiao, J.; Chen, X.; Sushko, P. V.; Sushko, M. L.; Kovarik, L.; Feng, J.; Deng, Z.; Zheng, J.; Graff, G. L.; Nie, Z.; et al. High-Performance LiNi 0.5Mn 1.5O 4 Spinel Controlled by Mn 3+ Concentration and Site Disorder. *Adv. Mater.* **2012**, *24*, 2109–2116. https://doi.org/10.1002/adma.201104767.

(42) Sushko, P. V.; Rosso, K. M.; Zhang, J. G.; Liu, J.; Sushko, M. L. Oxygen Vacancies and Ordering of D-Levels Control Voltage Suppression in Oxide Cathodes: The Case of Spinel LiNi0.5Mn1.5O 4-δ. *Adv. Funct. Mater.* **2013**, *23*, 5530–5535. https://doi.org/10.1002/adfm.201301205.

(43) Boulet-Roblin, L.; Villevieille, C.; Borel, P.; Tessier, C.; Novák, P.; Ben Yahia, M. Versatile Approach Combining Theoretical and Experimental Aspects of Raman Spectroscopy To Investigate Battery Materials: The Case of the LiNi 0.5 Mn 1.5 O 4 Spinel. *J. Phys. Chem. C* **2016**, *120*, 16377–16382. https://doi.org/10.1021/acs.jpcc.6b04155.

(44) Dokko, K.; Mohamedi, M.; Anzue, N.; Itoh, T.; Uchida, I. In Situ Raman Spectroscopic Studies of $LiNi_xMn_{2-x}O_4$ Thin Film Cathode Materials for Lithium Ion Secondary Batteries. *J. Mater. Chem.* **2002**, *12*, 3688–3693. https://doi.org/10.1039/B206764A.

(45) Amdouni, N.; Zaghib, K.; Gendron, F.; Mauger, A.; Julien, C. M. Magnetic Properties of LiNi0.5Mn1.5O4spinels Prepared by Wet Chemical Methods. *J. Magn. Magn. Mater.* **2007**, *309*, 100–105. https://doi.org/10.1016/j.jmmm.2006.06.018.

(46) Lee, E.; Persson, K. A. Revealing the Coupled Cation Interactions behind the Electrochemical Profile of LixNi0.5Mn1.5O4. *Energy Environ. Sci.* **2012**, *5*, 6047. https://doi.org/10.1039/c2ee03068c.

(47) Yoon, J.; Kim, D.; Um, J. H.; Jeong, M.; Oh, W.; Yoon, W.-S. Effect of Local Structural Changes on Rate Capability of LiNi 0.5 Mn 1.5 O 4−δ Cathode Material for Lithium Ion Batteries. *J. Alloys Compd.* **2016**, *686*, 593–600. https://doi.org/10.1016/j.jallcom.2016.06.044.

(48) Li, S. R.; Chen, C. H.; Dahn, J. R. Studies of LiNi0.5Mn1.5O4 as a Positive Electrode for Li-Ion Batteries: M3+ Doping (M = Al, Fe, Co and Cr), Electrolyte Salts and LiNi0.5Mn1.5O4/Li4Ti5O12 Cells. *J. Electrochem. Soc.* **2013**, *160*, A2166–A2175. https://doi.org/10.1149/2.075311jes.

(49) Lin, M.; Ben, L.; Sun, Y.; Wang, H.; Yang, Z.; Gu, L.; Yu, X.; Yang, X.-Q.; Zhao, H.; Yu, R.; et al. Insight into the Atomic Structure of High-Voltage Spinel LiNi 0.5 Mn 1.5 O 4 Cathode Material in the First Cycle. *Chem. Mater.* **2015**, *27*, 292–303. https://doi.org/10.1021/cm503972a.

(50) Muto, S.; Sasano, Y.; Tatsumi, K.; Sasaki, T.; Horibuchi, K.; Takeuchi, Y.; Ukyo, Y. Capacity-Fading Mechanisms of LiNiO2-Based Lithium-Ion Batteries. *J. Electrochem. Soc.* **2009**, *156*, A371. https://doi.org/10.1149/1.3076137.

(51) Streich, D.; Erk, C.; Guéguen, A.; Müller, P.; Chesneau, F. F.; Berg, E. J. Operando Monitoring of Early Ni-Mediated Surface Reconstruction in Layered Lithiated Ni-Co-Mn Oxides. *J. Phys. Chem. C* **2017**, *121*, 13481–13486. https://doi.org/10.1021/acs.jpcc.7b02303.

(52) Pieczonka, N. P. W.; Liu, Z.; Lu, P.; Olson, K. L.; Moote, J.; Powell, B. R.; Kim, J. Understanding Transition-Metal Dissolution Behavior in LiNi0.5Mn1.5O4 High-Voltage Spinel for Lithium Ion Batteries. *J. Phys. Chem. C 2013, 117, 15947−15957* **2013**.

(53) Qiao, R.; Wang, Y.; Olalde-Velasco, P.; Li, H.; Hu, Y.-S.; Yang, W. Direct Evidence of Gradient Mn(II) Evolution at Charged States in LiNi 0.5 Mn 1.5 O 4 Electrodes with Capacity Fading. *J. Power Sources* **2015**, *273*, 1120–1126. https://doi.org/10.1016/j.jpowsour.2014.10.013.

Table of Contents Image

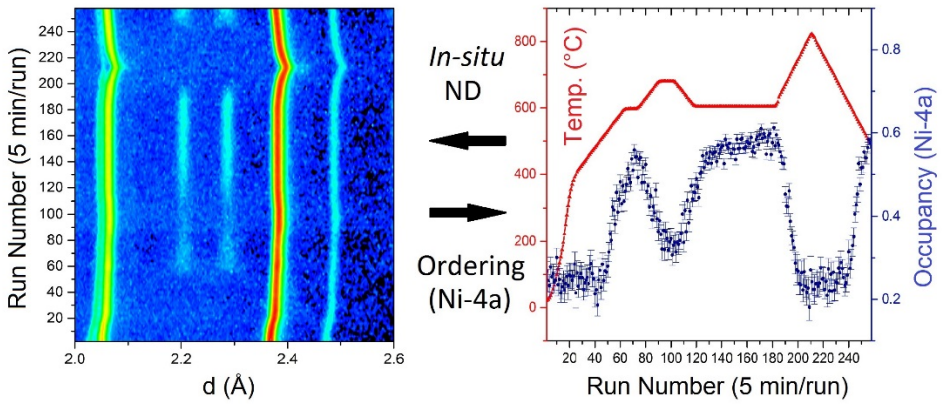
Run Number (5 min/run)
d (Å)
In-situ
ND
Ordering
(Ni-4a)
Temp. (°C)
Occupancy (Ni-4a)
Run Number (5 min/run)